

1 Effect of Cholesterol on Nano-Structural Alteration of Light-
2 Activatable Liposomes via Laser Irradiation: Small Angle
3 Neutron Scattering Study

4 Zheng Yuan, ‡^a Saikat Das, ‡^{a,#} Changwoo Do^b and Yoonjee C. Park^a

5
6
7 ^aDepartment of Chemical & Environmental Engineering, University of Cincinnati, Cincinnati,
8 OH 45220

9 ^bNeutron Scattering Division, Oak Ridge National Laboratory, Oak Ridge, TN 37831

10 # Current address: Intel Corporation, Hillsboro, OR 97124

11 ‡ These authors contribute equally to this work.

12
13
14 **Abstract**

15 Although the light-activated liposomes have been extensively studied for drug delivery
16 applications, the fundamental mechanism of the drug release based on lipid compositions has not
17 been fully understood. Especially, despite the extensive use of cholesterol in the lipid
18 composition, the role of cholesterol in the light-activated drug release has not been studied. In
19 this study, the influence of cholesterol on drug release from light-responsive drug-encapsulated
20 liposomes after activated by near infrared (NIR) laser was investigated. We prepared
21 methotrexate (MTX)-encapsulated DSPC liposomes consisting of 0 mol% (–Chol) or 35 mol%
22 cholesterol (+Chol), with (+Au) or without gold nanorods (–Au) on the lipid bilayer to compare
23 drug release, morphological changes, and nanostructures after laser irradiations. Transmission
24 electron microscopy (TEM) and small angle neutron scattering (SANS) data revealed that only
25 +Chol +Au liposomes showed partial aggregation of the liposomes after laser irradiation. Similar
26 trends on the drug release and structural change were observed when the liposomes were heated
27 to above chain-transition temperature. Overall, we have found that (1) inclusion of 35 mol%
28 cholesterol enhanced the permeability of lipid bilayers above T_c ; (2) the mechanism of laser-
29 activated liposomal drug delivery is disrupting lipid bilayer membranes by the photothermal
30 effect in the presence of plasmonic materials. By understanding the fundamentals of the
31 technology, precise controlled drug release at a targeted site with great stability and repeatability
32 is anticipated.

1 1. Introduction

2 Liposomes have been proposed as carriers for drug delivery since 1970s¹. Liposomes are
3 one of the most widely used drug delivery materials because of inherent biocompatibility, low
4 toxicity and ability to encapsulate both hydrophilic and hydrophobic drugs. Liposomes have
5 been produced by various methods, including probe-sonication,² extrusion,³ reverse-phase
6 evaporation,^{4, 5} and recently developed supercritical fluid method.^{6,7} Because passive delivery
7 of encapsulated drugs from liposomes has often limited the efficacy,⁸ liposomes have been
8 recently engineered to release encapsulated drugs on the target of interest in a controlled fashion
9 in response to external stimuli such as pH, light, and high temperature.⁹

10 In recent years, laser-activatable liposomes with gold nanoparticles as a plasmonic
11 photothermal agent have been investigated extensively for on-demand drug release^{10 11 12 13}.
12 This type of liposomes offered a novel method to control drug release at the targeted sites with
13 the laser source as a precise switch.¹⁴ Although the light-activated liposomes have been
14 extensively studied because of its advantage, few applications have been tested in clinical trials
15 and only one is approved by FDA.¹⁵ The use of light-activated liposomal drug delivery systems
16 will be widely applied if the amount of drug is precisely controlled at a target location with great
17 stability. In order to achieve the goal of translating the technology to clinical settings, the
18 fundamentals of the light-activated liposomal drug delivery need to be understood based on the
19 lipid compositions and mechanisms. The drug release mechanism is considered as the following.
20 When the liposomes triggered by laser, the lipid membrane is locally heated to above the chain-
21 transition temperature via plasmon surface resonance of gold nanoparticles. During this process,
22 the permeability of the local or whole lipid bilayer may change to allow the encapsulated drug to
23 diffuse through the membrane. For the lipid composition, in addition of phospholipids,
24 cholesterol has been studied and utilized in liposomes for drug release, mainly regarding its
25 ability to stabilize the formulations.¹⁶ However, effect of cholesterol in light-activatable
26 liposomes on controlling drug release remains unclear.

27 In this study, we will examine the role of cholesterol in drug release as well as
28 morphological changes using transmission electron microscopy (TEM) and small-angle neutron
29 scattering (SANS) analysis to identify the fundamentals. Previously we fabricated gold nanorod
30 (AuNR)-coated liposomes containing 35 mol% cholesterol (+Chol +Au) and showed that these
31 liposomes released drug repetitively with multiple laser cycles.^{17 18} Because cholesterol also
32 plays a role in adjusting lipid bilayer permeability,^{19 20 21 22} we hypothesize that if the drug
33 release mechanism of light-activatable liposomes is the permeability change by heating,
34 cholesterol will impact drug release amount. In addition, the morphological changes in the nano-
35 scale may indicate the reorganization of the lipids in the bilayer after “chain-melting” via the
36 photothermal effect. Lastly, we studied the effect of bulk heating to 75 °C (above T_c) on drug
37 release and structural changes, to compare with the irradiated liposomes, which are spatially
38 heated. Thus, this study will advance fundamental understandings in how cholesterol affects the

1 lipid membranes and tunes drug release of light-responsive liposomes upon laser irradiation. The
2 results will also support drug release mechanism and promote applications of laser-controlled
3 nanomedicine.

4

5 **2. Materials and Methods**

6 **2.1 Materials**

7 Cholesterol was purchased from Sigma-Aldrich (St. Louis, MO). 1,2-distearoyl-sn-
8 glycerol-3-phosphocholine (DSPC) and 1,2-Distearoyl-sn-glycerol-3-phosphoethanolamine-N-
9 [methoxy(polyethylene glycol)-5000] (DSPE-PEG 5000) were obtained from Avanti Lipids
10 ((Alabaster, AL). Potassium chloride and deuterium oxide (D₂O, 99.8 atom %D) were purchased
11 from Fisher Scientific (Waltham, MA). The rest of the materials used in this study was
12 mentioned in our previous publication.¹⁷ An aqueous citrate-capped gold nanorod dispersion
13 with average size of 10 nm × 59 nm was purchased from Nanopartz, Inc. (Loveland, CO).

14

15 **2.2 Synthesis of light-activatable liposomes**

16 Briefly, the AuNR-attached liposomes were fabricated by a probe-sonication method as
17 previously described¹⁷. For preparing liposomal formulations with and without cholesterol, DSPC,
18 cholesterol, stearylamine and DSPE-PEG 5000 were dissolved in chloroform and mixed at two
19 molar ratios, 50:35:10:5 (+Chol) and 85:0:10:5 (−Chol), respectively. 10 μmol of total lipids
20 amount were kept constant for each mixture. After lipids were completely dried overnight in a
21 fume hood at room temperature, 2 mL of D₂O was added and sonicated for 10 min × 3 cycles to
22 form liposomes. D₂O was used to have contrast variation between the solvent/core and the
23 liposomes bilayer in the EQ-SANS experiments. The liposome suspension was then centrifuged
24 twice, at 4000 rpm × 30 min followed by 6000 rpm × 20 min, to increase the final lipid
25 concentration to 84.6 mg/mL. AuNRs (4.7×10¹³/mL) were tethered on the liposomal membranes
26 via electrostatic attractions by mixing the AuNR suspension with the liposome suspension.

27 To prepare drug-loaded liposomes for laser-triggered release tests, liposomes were
28 prepared via the same method with methotrexate (MTX) solution (2 mL, 25 mg/mL dissolved in
29 DI water) substituted for D₂O. Unencapsulated MTX was removed by a dialysis device prior to
30 drug releasing tests.¹⁷

31

32 **2.3. Dynamic light scattering (DLS) and Zeta potential**

33 The average liposome/nanodroplet size and size distribution was determined using
34 dynamic light scattering (NanoBrook Omni, Brookhaven Instruments, Holtsville, NY, USA). 20

1 μL of gold nanorod-coated liposomes was diluted 50 times in DI water and measurements were
2 repeated three times for a period of 60 seconds each at room temperature at a reading angle of 90° .
3 The zeta potential was measured using the same instrument with an electrode provided in the same
4 condition as the DLS measurement.

5 **2.4 Transmission Electron Microscope (TEM)**

6 The TEM images of the liposomes before and after laser irradiations were obtained as
7 described previously^{17, 18}. Briefly, liposomal samples were treated with 0 sec or 20 sec laser
8 irradiations. Subsequently, $10\times$ diluted samples were applied on a formvar/carbon-coated grid and
9 negatively stained with 2% uranyl acetate. Then the samples on the TEM grid were lyophilized in
10 a FreeZone Freeze Dry system (Kansas City, MO) and immediately imaged.

11 **2.5 ImageJ Analysis**

12 TEM images were analyzed by ImageJ software²³ to estimate the sizes and polydispersity
13 of AuNR, Au spheres and liposomes. For AuNR or Au spheres, the sizes are measured manually.
14 After the scale was set for each TEM image, each Au nanoparticle was selected and measured
15 three times to get an average value of the sizes. For liposomes, the area measurements were done
16 by both automatic counting and manual counting. First, the TEM images were converted to binary
17 images after adjusting the threshold. After selecting a proper size cutoff and circularity (above
18 0.2), each disjoint liposome in the image can be automatically outlined and measured using the
19 command of *Analyze Particles*. The results of sphere areas were exported, and the mean radii and
20 polydispersity (PD) were calculated correspondingly. Meanwhile, tightly packed liposomal
21 clusters or deformed liposomes were considered as aggregates, and they can't be accurately
22 recognized or measured by the *Analyze particles* command. Thus the individual liposomes in a
23 cluster were manually measured three times to obtain the average radius ($R_{liposome}$). The radius
24 of an aggregate ($R_{aggregate}$) was calculated via:

$$25 V_{shell, individual liposome} = \frac{4}{3}\pi R_{liposome}^3 - \frac{4}{3}\pi (R_{liposome} - d_t)^3 \quad (1)$$

$$26 V_{shell, aggregate} = \sum V_{shell, individual liposome} = \frac{4}{3}\pi R_{aggregate}^3 \quad (2)$$

27 where $R_{liposome}$ is the average radius of liposome measured by ImageJ, d_t is the shell thickness
28 (4.3 nm for non-irradiated sample and 4.5 nm for laser-irradiated sample), V_{shell} represents the
29 volume of the lipid shell for liposome or aggregate. The ImageJ analysis was performed based on
30 approximately 500 liposomes in multiple TEM images.

31 **2.6 Laser-triggered repetitive drug release tests**

32 The liposomes were irradiated following a procedure mentioned previously.^{17, 18} Briefly,
33 the liposome suspension was loaded in a glass capillary and irradiated with 1 to 4 cycles (5 sec per
34 cycle) at 1.1 Watts by a near infrared pulse laser beam (wavelength: 1064 nm; pulse repetition
35
36

1 frequency: 10kHz). The glass capillary is fully covered by the beam upon irradiation experiments
2 to ensure all the liposomes are irradiated upon each cycle. The released amount of MTX from
3 irradiated liposomes was determined using a UV-vis spectrometer as described previously.¹⁷
4

5 **2.7 Heating-triggered drug release tests**

6 The MTX-encapsulated liposome suspensions were placed in a water bath at 75°C for 15
7 minutes. After heating, the samples were cooled to room temperature and diluted 20 × using DI
8 water. Samples were then stored at room temperature for 18 hours. The released amount of MTX
9 was determined using a UV-vis spectrometer as described in previous work.¹⁷
10

11 **2.8 Small angle neutron scattering (SANS)**

12 SANS measurements were performed at the extended q -range small angle neutron scattering
13 diffractometer (EQ-SANS) of the Spallation Neutron Source (SNS) at Oak Ridge National
14 Laboratory (ORNL). A single instrument configuration with 4 m sample to detector distance was
15 used for all experiments. Frame-skipping (30 Hz) was used to have two bandwidths of 2 Å-5.7 Å
16 and 9.3 Å-13.0 Å, resulting a q -range of 0.004 Å⁻¹- 0.44 Å⁻¹²⁴. The neutron scattering data was
17 reduced by a standard procedure implemented in Mantid Plot²⁵. During this procedure the
18 collected data was corrected for open beam neutron flux and background scattering. The data was
19 then circularly and annularly averaged to produce scattering intensity (I) profile as a function of
20 scattering vector q ,

$$21 \quad q = \frac{4\pi}{\lambda} \sin(\theta) \quad (3)$$

22 where θ is the scattering angle and λ is the neutron wavelength.

23 The measured scattering intensity is modeled by

$$24 \quad I(q) = n\Delta\rho^2V^2P(q)S(q) + I_{inc} \quad (4)$$

25 where n is the number density of liposomes, $\Delta\rho$ is the difference in the scattering length density
26 between the solvent and the liposomal shells, V is the volume of the liposome shells, $P(q)$ is the
27 form factor corresponding to the internal structures of liposomes, and $S(q)$ is the structure factor
28 that described the inter-particle interactions. For a diluted system such as this study, $S(q)$ is
29 considered as 1. I_{inc} is the incoherent background.

30 Total 90 μL of liposomes solution that was prepared in D₂O was irradiated by above
31 mentioned laser irradiation method in 3 capillaries. The irradiated liposomes solution was collected

1 and was diluted 4 times using D₂O. The liposomes solution was placed inside a banjo-style cuvette
2 with 1 mm path length and 350 µl total liquid volume. All the EQ-SANS measurements were then
3 done at room temperature (~25°C).

4

5 **3. Results and Discussion**

6 **3.1 Effect of cholesterol on laser-triggered drug release**

7 The characterization of the liposomes is described in our previous publication.¹⁷ Briefly,
8 the size was 149.53 ± 6.18 nm with a polydispersity index (PDI) of 0.18 ± 0.04 for -Chol -Au
9 (no cholesterol and no gold nanorods) liposomes, and 155.34 ± 2.57 nm with a PDI of $0.15 \pm$
10 0.08 for +Chol -Au liposomes, according to the dynamic light scattering (DLS) data. The zeta
11 potential value was 3.08 ± 1.82 mV for the -Chol -Au liposomes and 3.06 ± 1.52 mV for the
12 +Chol -Au liposomes. The positive values were designed for electrostatic binding of negatively
13 charged citrate-coated AuNRs on the liposome surface. The p-values for the size and zeta
14 potential between -Chol -Au and +Chol -Au were 0.90 and 0.99, respectively, implying no
15 statistically significant difference. TEM data analysis provided additional morphological
16 information, including location of AuNR on the liposomes and the size distribution, which will
17 be discussed in section 3.2 in details.

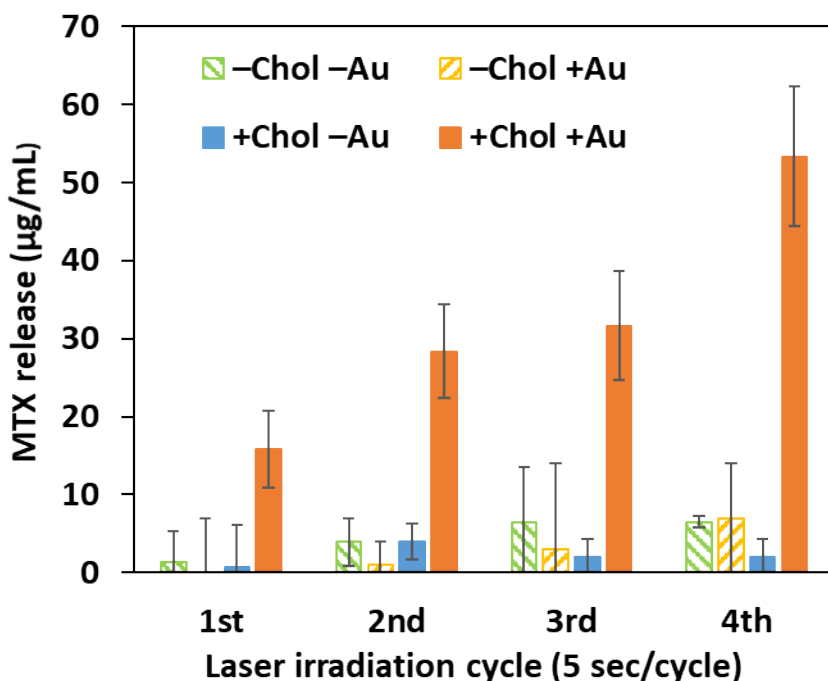
18 Figure 1 shows the effect of cholesterol and AuNR on total MTX release as a function of
19 the number of laser irradiation cycles (5 sec each cycle). +Chol +Au liposomes showed that the
20 amounts of total MTX released after the 1st, 2nd, 3rd, and 4th cycles were 15.8 ± 5.0 , 28.3 ± 6.0 ,
21 31.6 ± 7.0 and 53.3 ± 7.0 µg/mL respectively. The difference between these MTX releases with
22 respect to irradiation cycles were statistically significant ($p < 0.05$), except the 2nd and 3rd
23 cycles ($p=0.253$) (Supplementary Table S1). The results indicate that the MTX release was
24 proportional to the number of laser irradiation cycle. The MTX released of +Chol +Au liposomes
25 at each cycle was significantly higher than other groups.

26 The amount of total MTX released from +Chol -Au liposomes after the 1st, 2nd, 3rd, and
27 4th cycles were 0.7 ± 5.4 , 3.9 ± 2.3 , 2.0 ± 2.3 and 2.0 ± 2.3 µg/mL respectively. The MTX releases
28 with respect to irradiation cycles were not significantly different ($p > 0.05$ for all pairs.
29 Supplementary Table S2). The results suggest strong surface plasmon heating of AuNR on MTX
30 release from +Chol liposomes after laser irradiation cycles.

31 In the case of -Chol -Au liposomes, the total amount of MTX released after the 1st, 2nd, 3rd,
32 and 4th irradiation cycles were 1.3 ± 4.0 , 3.9 ± 3.0 , 6.5 ± 7.0 , 6.5 ± 0.8 µg/mL, respectively. The
33 difference of these MTX releases between irradiation cycles were not statistically significant for
34 all ($p > 0.05$ for all pairs. Supplementary Table S3). -Chol +Au liposomes released 0.0 ± 7.0 ,
35 1.0 ± 3.0 , 3.0 ± 11.0 and 7.0 ± 7.0 µg/mL after the 1st, 2nd, 3rd, and 4th irradiation cycles,

1 respectively. The p values between all pairs were greater than 0.05 (Supplementary Table S4),
2 demonstrating that the MTX release was not significantly affected by laser irradiation without
3 cholesterol in the liposome composition. The differences between total MTX released between
4 -Chol -Au and -Chol +Au liposomes at each cycle were also not statistically significant,
5 according to the t-test ($p > 0.05$ for all pairs. Supplementary Table S5).

6 By comparing the MTX releases between -Chol +Au and +Chol +Au group at each cycle ($p <$
7 0.05 for all pairs. Supplementary Table S6), we found that the presence of cholesterol was of
8 crucial importance for the drug release of these liposomes when activated by laser. This is in
9 agreement with other study²⁶, in which García et al. found that AuNP-anchored liposomes
10 containing 40 mol% cholesterol reached higher release amount than those with only 3.35 mol%
11 cholesterol at temperature higher than T_c . They proved that increasing temperature from 37°C
12 above T_c enhanced the drug release ability for AuNP-liposomes with 40 mol% of cholesterol²⁶.
13 Note that the opposite phenomenon was also reported previously. Jeong Eun Shin et al.²⁷ has
14 reported that hollow gold nanoshell conjugated-DPPC liposomes with 40% Chol possessed a
15 higher threshold of light power to release payload than cholesterol-free liposomes. One reason
16 that possibly leads to the contradictory findings is the difference in triggering mechanism. Shin
17 et al. has attributed the payload release to the transient nanobubbles formed by the hollow gold
18 nanoshells upon laser exposure, which caused mechanical lysing of liposomes^{27 28}.



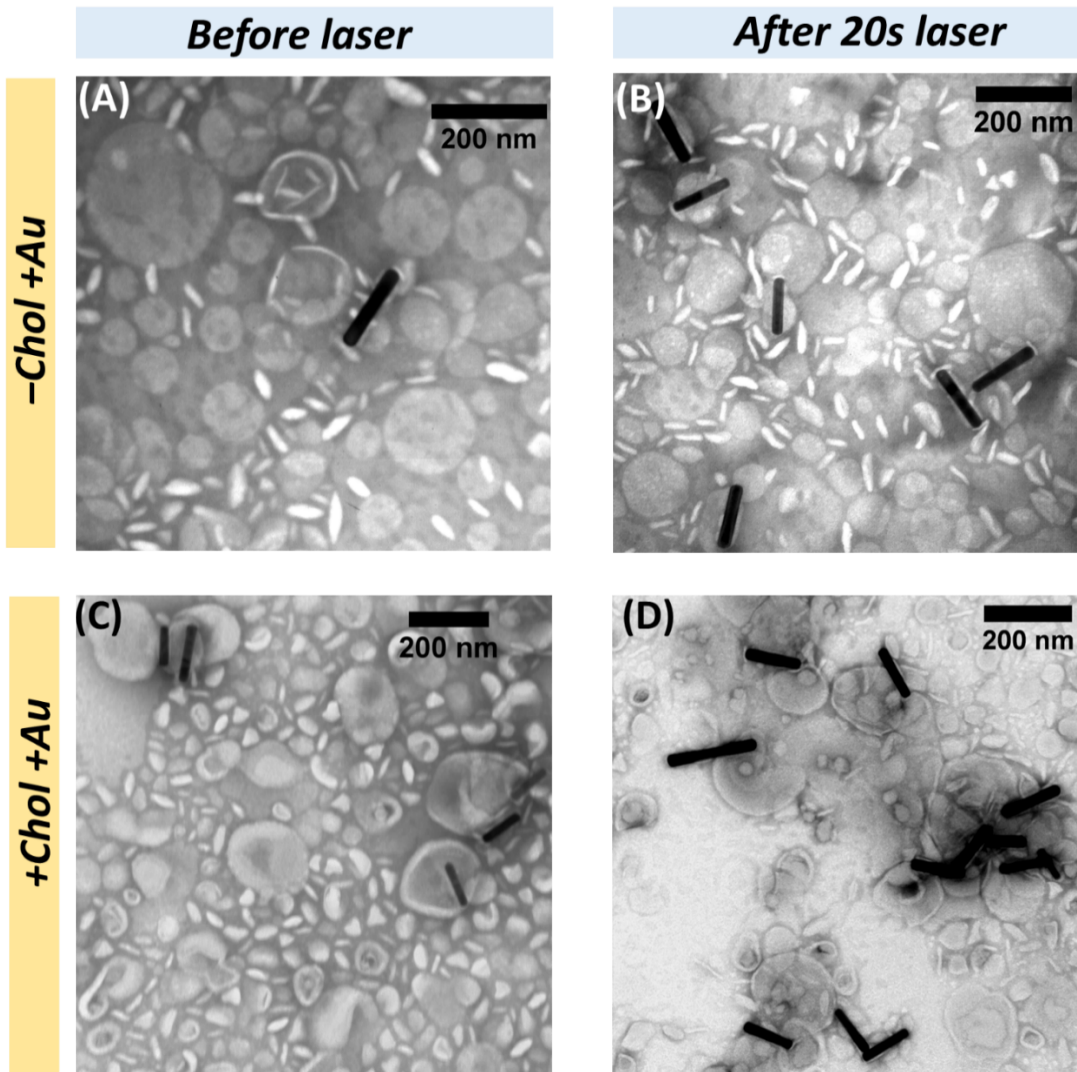
19
20 Figure 1. Laser-triggered MTX release measurement for -Chol -Au liposomes (hatched green), -Chol
21 +Au liposomes (hatched yellow), +Chol -Au liposomes (solid blue) and +Chol +Au liposomes (solid

1 orange) after 1 to 4 laser cycles (5 sec laser irradiation per cycle, 3 min cooling time between each cycle)
2 at 1.1 W.

3

4 **3.2 Effect of Cholesterol on morphological changes upon irradiation**

5 The morphological changes of the light-activated liposomes, -Chol +Au and +Chol +Au
6 liposomes, upon laser irradiation were examined by TEM. Some liposomes appeared to be an
7 ellipsoidal shape due to potential collapse during the freeze-drying process of the TEM sample
8 preparation. Figure 2A and Figure 2B show the TEM images of -Chol +Au liposomes before
9 irradiation and after laser irradiation, respectively. No visible changes were observed. In contrast
10 to the -Chol +Au liposomes, laser-irradiated +Chol +Au liposomes showed notable changes
11 (Figure 2D). Some +Chol +Au liposomes aggregated, deformed, and seemed fused, especially
12 near the AuNR. Figure S1 in Supplementary also showed the trend. In addition, some gold
13 nanospheres were also observed, indicative of the melting of AuNR (Figure S1). DLS
14 measurements were also conducted to characterize the size change of +Chol +Au liposomes
15 before and after laser. However, no significant changes of hydrodynamic diameter were found
16 (Supplementary Figure S2). Interestingly, the size distribution shifted to the right (regime of
17 larger size) after the laser irradiation, but the average diameter was unchanged.

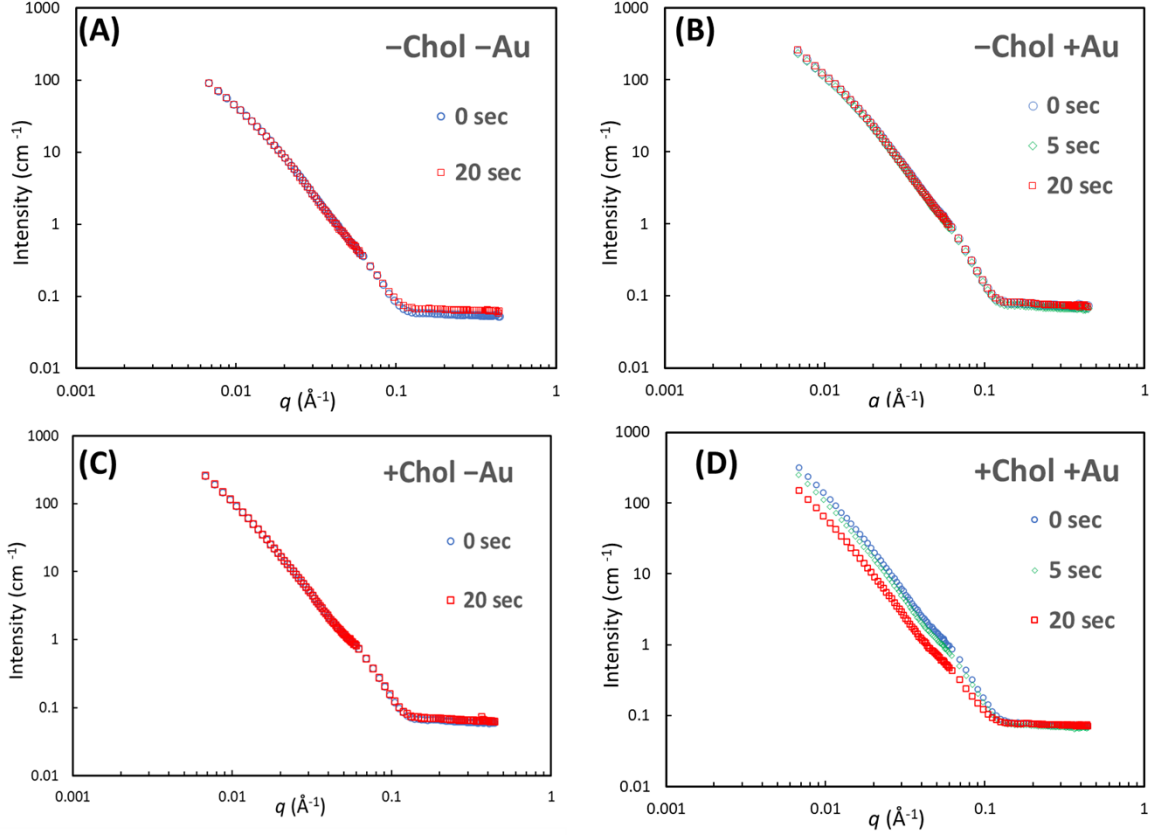


1
 2 Figure 2. TEM images of (A)–Chol +Au liposomes before laser irradiation and (B) after 20 sec (5 sec × 4
 3 cycles) laser, (C) +Chol +Au liposomes before laser irradiation and (D) after 20 sec (5 sec × 4 cycles)
 4 laser.

5
 6 **3.3 Effect of cholesterol on nanostructures**
 7 **3.3.1 Effect of laser**

8 The EQ-SANS curves for all liposome formulations with different laser irradiation
 9 durations are presented in Figure 3. Besides +Chol +Au liposomes (Figure 3D), all the other
 10 formulations (–Chol –Au, +Chol –Au, –Chol +Au) showed no remarkable changes between no
 11 laser and with laser. +Chol +Au exhibited a curve shift from high q to low q with increased laser

- 1 irradiation durations, which was revealed by the slope change at q range of $0.04 \text{ \AA}^{-1} \sim 0.1 \text{ \AA}^{-1}$. It
- 2 indicates a size increase after laser irradiation, which will be discussed later in details.



3
 4 Figure 3. EQ-SANS scattering curves for (A) –Chol –Au liposomes with 0 sec or 20 sec laser, (B) +Chol
 5 –Au liposomes with 0 sec or 20 sec laser, (C) –Chol +Au liposomes with 0 sec, 5 sec or 20sec laser, (D)
 6 +Chol +Au liposomes with 0 sec, 5 sec or 20 sec laser.

7 We first evaluated the bilayer thicknesses through the Kratky-Porod approximation based
 8 on the range from $0.001 \text{ \AA}^2 < q^2 < 0.006 \text{ \AA}^2$ ^{29, 30}. The equations are:

9
$$I(q) = I(0)q^{-2}\exp(-R_t^2q^2) \quad (5)$$

10
$$I_{exp}(q)q^2 = I(q)q^2 + I_{inc}q^2 \quad (6)$$

11 where R_t is the radius of gyration of the bilayer, $I_{exp}(q)$ is the experimental scattering intensity,
 12 and the I_{inc} is the incoherent scattering. Hence, by plotting $\ln [I(q) \cdot q^2]$ as a function of q^2
 13 (Figure 4), the lamellar radius of gyration R_t was obtained from the slope of a linear regression.

1 Note that the scattering background I_{inc} has been subtracted from the scattering intensities prior
2 to plotting. The bilayer thickness can be estimated via:

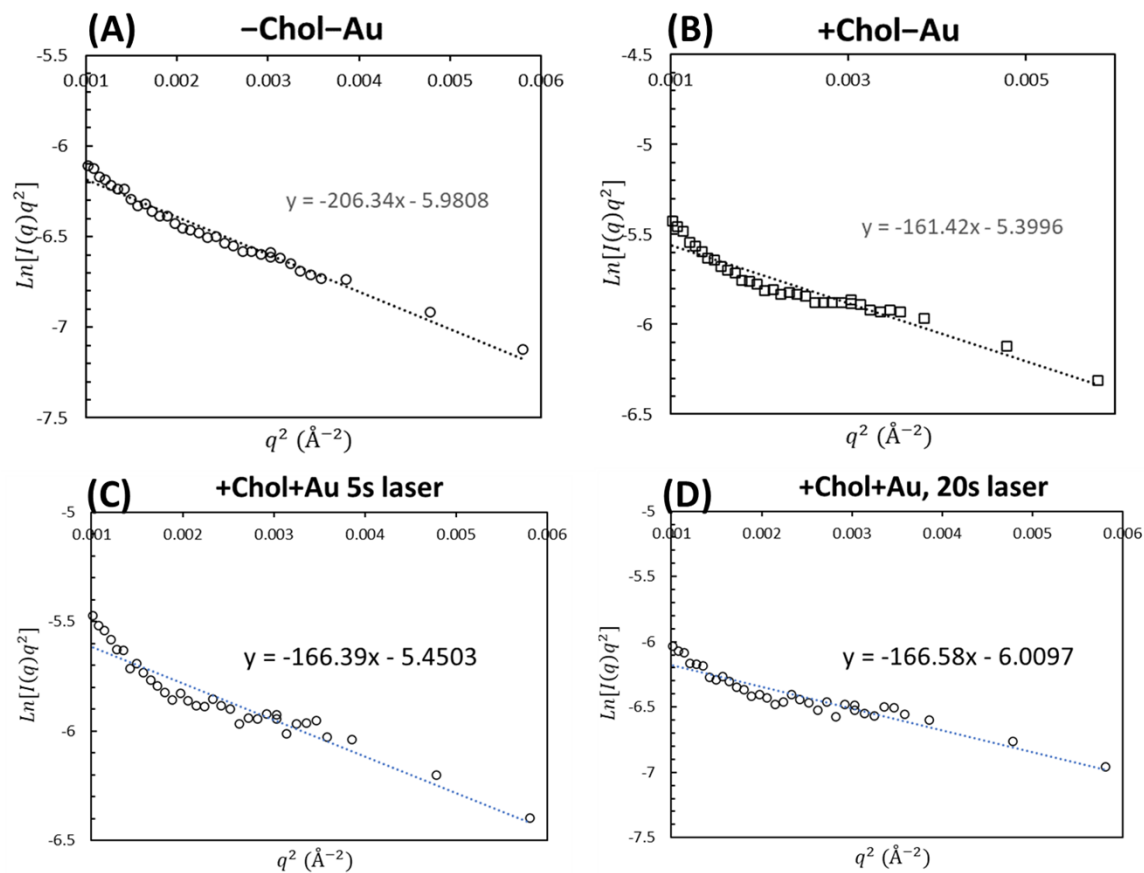
$$3 \quad d_t^2 \cong 12R_t^2 \quad (7)$$

4 The bilayer thicknesses obtained from the Kratky-Porod plots are summarized in Table 1. For
5 -Chol -Au liposomes, the bilayer thickness was determined to be 5.0 ± 0.1 nm, which is which is
6 in agreement with 5.1 nm that was previously reported elsewhere ³¹. Addition of 35 mol%
7 cholesterol decreased the bilayer thickness to 4.4 ± 0.1 nm. This is likely caused by the kink or
8 deformation of the hydrocarbon chains of the DSPC lipids to accommodate the cholesterol
9 molecules ³². It is also noteworthy that the effect of adding cholesterol on bilayer thickness depend
10 on the acyl chain lengths of the lipids. For saturated phosphatidylcholines with shorter chains, e.g.,
11 12 to 16 carbons, inclusion of certain amount of cholesterol was found to increase the bilayer
12 thickness ^{29,32}. After 5 sec or 20 sec laser irradiation, +Chol +Au liposomes showed a thickness of
13 ~4.5 nm.

14

15

16



1

Figure 4. The Kratky-Porod plots of the EQ-SANS scattering data for (A) -Chol -Au, (B)+Chol -Au, (C) +Chol +Au after 5 sec laser irradiation, and (D) +Chol +Au after 20 sec laser irradiation. Dashed lines are the trendlines of linear fittings.

2

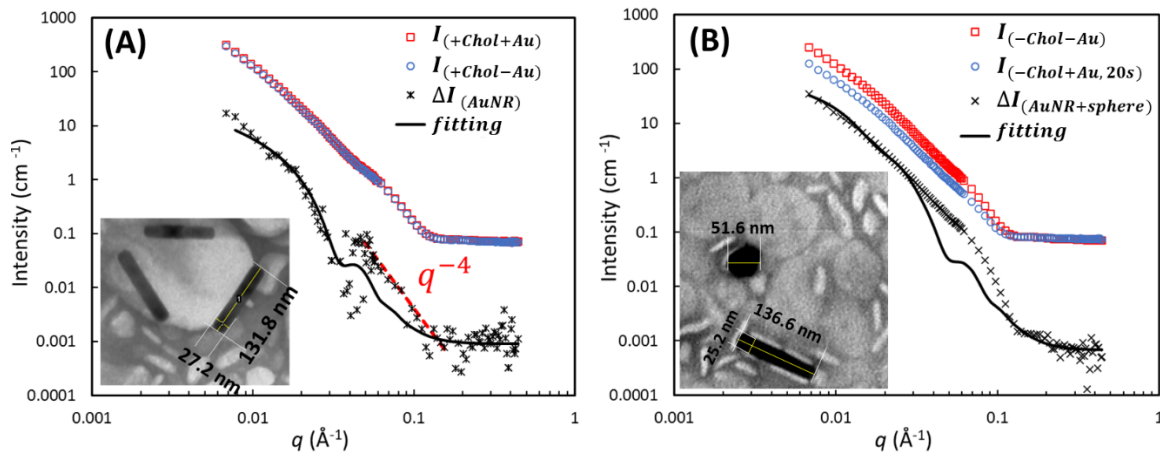
3 Table 1. Parameters of the lipid bilayers for different liposomes obtained from the Kratky-Porod plots.

Composition	R_t^2 (nm ²)	d_t (nm)
-Chol-Au	2.1 ± 0.1	5.0 ± 0.1
+Chol-Au	1.6 ± 0.1	4.4 ± 0.1
+Chol +Au, 5 sec laser	1.7 ± 0.1	4.5 ± 0.1
+Chol +Au, 20 sec laser	1.7 ± 0.1	4.5 ± 0.2

4

1 Before proceeding to model fitting, we examined the structures of AuNR in the scattering
 2 curves by intensity subtraction. As shown in Figure 5A, by subtracting the scattering curve I
 3 $(+Chol - Au)$ from the curve $I (+Chol + Au)$, the residual intensity theoretically only contained the
 4 structure information of AuNR. By fitting the residual intensity ΔI with a cylinder model, we
 5 found that the fitting yields a 11 nm (radius of cross section) \times 132 nm (length) rod structure
 6 (Table 2). This is in agreement with the average size of AuNRs observed in TEM images (shown
 7 in Figure 5A inset). The polydispersity index used in fitting were obtained from ImageJ analysis
 8 of TEM images (Supporting Information, Table S8).

9 Next, we examined AuNR structures solely after laser irradiation. By subtracting $I (-Chol$
 10 $- Au)$ from $I (-Chol + Au, 20 \text{ sec})$, we can extract the AuNR structures that were exposed to 20sec-laser
 11 irradiation (Figure 5B). According to TEM images (Figure 5B inset and Figure S1), a portion of
 12 AuNRs melted and formed Au spheres after 20 sec-laser. Thus, the ΔI curve was fitted with a
 13 customized model consisting of a sphere-model and a cylinder-model, representing the Au
 14 spheres and AuNRs respectively. The fitting curve slightly deviated at the q range of 0.04 \AA^{-1}
 15 $\sim 0.1 \text{ \AA}^{-1}$, probably because of liposomes in the subtracted curve. The fitting parameters of the
 16 combined model are presented in Table 2, suggesting the co-existence of Au spheres with a
 17 radius of 22.8 nm and AuNRs with a size of 11 nm \times 132 nm. This result is consistent with the
 18 sizes of AuNR and Au spheres measured in TEM images (Figure 5B inset).



19

20 Figure 5. The subtracted scattering curves and the corresponding fittings. (A) AuNR residual intensity
 21 obtained by subtracting $I(+Chol - Au)$ from $I(+Chol + Au)$. (B) AuNR and Au sphere residual intensity obtained by
 22 subtracting $I(-Chol - Au)$ from $I(-Chol + Au, 20 \text{ sec laser})$; the ΔI curve has been shifted for better illustration. Insets
 23 showed the corresponding TEM images of AuNR or Au sphere structures.

24

1 Table 2. Fitting parameters for the ΔI curves in Figure 5 (A) and (B), respectively.

Figure	5(A)	5(B)
Fitting Model (component)	Cylinder (AuNR)	Cylinder (AuNR) + Sphere (Au sphere)
Size (nm)	AuNR: 11 (radius) \times 132 (length)	AuNR: 11 (radius) \times 132 (length) Au sphere: 22.8 (radius)
PD ^a	0.14 (radius, AuNR)	0.20 (length, AuNR) 0.12 (radius, Au sphere)

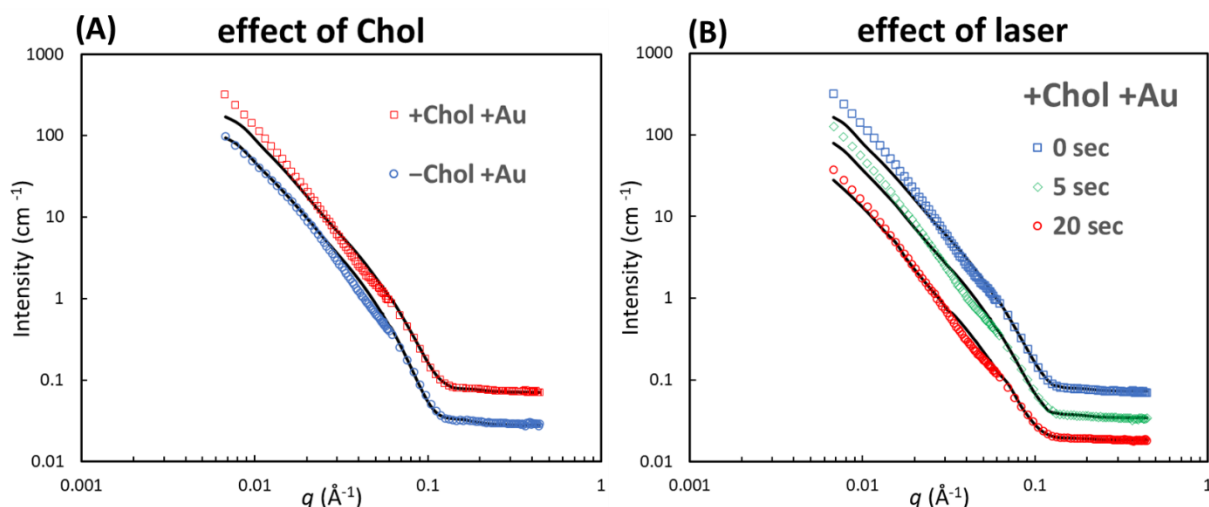
2 ^aPD represents polydispersity. PD values were obtained from TEM image analysis.

3

4 Combination of a core-shell-sphere model and AuNR/Au spheres was used to fit the
 5 liposomes, based on the volume fraction of the particles (Figure 6A and Table 3). For simplicity,
 6 only fitting parameters for the +Au groups are shown. The fittings on -Chol -Au and +Chol
 7 -Au liposomes shared the same parameters with -Chol +Au and +Chol +Au on the part of core-
 8 shell-sphere model, respectively. The polydispersity obtained from TEM image analysis (Table
 9 S8) was used for fitting. For the +Chol +Au data with 5 sec or 20 sec laser, as discussed in
 10 section 3.2, there was no overall size increase observed by DLS. Thus, a second core-shell-
 11 sphere model with bigger size was used for the laser irradiated aggregated/fused liposomes
 12 samples.

13 The fittings of the scattering curve of the +Chol +Au liposomes with 5 sec laser (Table 3)
 14 showed liposomal aggregates with a radius of ~230 nm. The volume fraction (represented by scale)
 15 of the original population of liposomes decreased from 0.06 to 0.049, suggesting about 19% of
 16 original liposomes aggregated/fused. Moreover, the fitting parameters of the +Chol +Au with 20
 17 sec laser suggested that the size of liposomal aggregate remained at 230 nm while the fraction of
 18 original liposomes further decreased from 0.049 to 0.027. This indicates approximately 56% of
 19 liposomes aggregated with longer laser duration. Note that the volume fraction percentage is based
 20 on lipid volume, excluding water core in the liposomes.

21 Overall, the fitting results suggested that a portion of liposomes aggregated after laser
 22 irradiation accompanied with melting of some AuNRs and with no significant changes in the
 23 lipid bilayer thickness. This result is in good agreement with the morphological changes
 24 observed by TEM and the Kratky Plot results. Despite of some deviations in the fitting curves,
 25 the combined custom model described the shift of the scattering curves with different irradiation
 26 durations.



1
 2 Figure 4. EQ-SANS scattering curves for (A) +Chol +Au liposomes and -Chol +Au liposomes, showing
 3 the difference caused by inclusion of cholesterol. (B) +Chol +Au liposomes with 0 sec, 5 sec or 20sec
 4 laser, respectively, showing the changes caused by laser irradiation. The black solid lines are
 5 corresponding fitting curves. Some scattering curves are shifted vertically for better illustration.

6
 7 Table 3. Fitting models and parameters for the -Chol +Au liposomes, +Chol +Au liposomes with 0 sec, 5
 8 sec or 20 sec laser irradiation, respectively.

Sample	Model (component)	d_t (nm)	R_{core} (nm)	PD	Scale	Percentage of liposome/aggregate
-Chol +Au	Core-shell-sphere (liposome)	5.0	47	0.30	0.060	100% liposome
	Cylinder (AuNR)	Radius \times Length: 13 \times 132		0.14 (radius) 0.20 (length)	0.005	
+Chol +Au	Core-shell-sphere (liposome)	4.3	51	0.27	0.060	100% liposome
	Cylinder (AuNR)	Radius \times Length: 13 \times 132		0.14 (radius) 0.20 (length)	0.005	
+Chol +Au	Core-shell-sphere (liposome)	4.5	51	0.30	0.049	81% liposome
5 sec laser	Core-shell-sphere (aggregate)	4.5	230	0.50	0.011	19% aggregate

	Cylinder (AuNR)	Radius × Length: 13 × 132		0.14 (radius) 0.20 (length)	0.0045	
	Sphere (Au Sphere)	Radius: 23		0.12	0.0005	
	Core-shell-sphere (liposome)	4.5	51	0.50	0.027	
+Chol +Au	Core-shell-sphere (aggregate)	4.5	230	0.50	0.033	44% liposome
20 sec laser	Cylinder (AuNR)	Radius × Length: 13 × 132		0.14 (radius) 0.20 (length)	0.004	56% aggregate
	Sphere (Au Sphere)	Radius: 23		0.12	0.001	

1 The discrepancy between DLS and the SANS data or the TEM data have been reported
2 elsewhere.³³ We suspect that it is because of the sample preparation step for the DLS
3 measurement, which requires dilution of the sample for a sufficient volume, resulting in the
4 breakdown of the aggregates. It implies that the aggregation is likely to be reversible. This
5 hypothesis also supports our previous finding that the number density of liposomes didn't change
6 before and after laser irradiation when being measured in a highly diluted condition by an
7 ultramicroelectrode.¹⁷

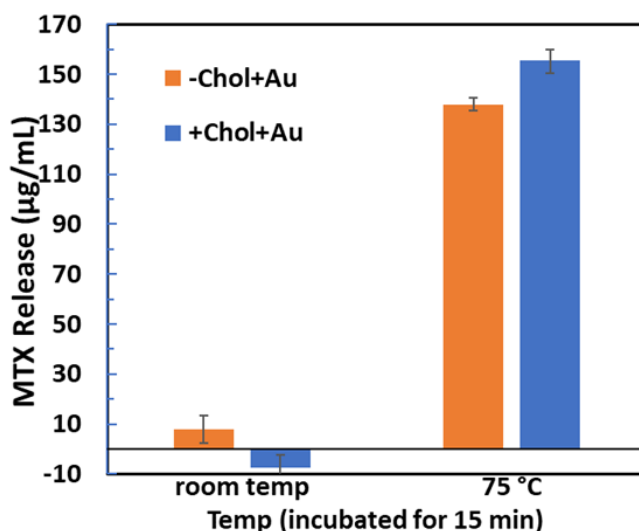
8

9 3.3.2 Effect of heating

10 The effect of heating on the drug release and structural changes of liposomes were
11 examined. Figure 7 shows that -Chol +Au and +Chol +Au liposomes released 7.9 ± 5.5 $\mu\text{g/mL}$
12 and -7.6 ± 4.6 $\mu\text{g/mL}$ MTX, respectively ($p = 0.006$), during 18 hours at room temperature. The
13 results suggest that cholesterol does not play a role in drug release at temperature below T_c .
14 Similarly, many previous studies have shown that cholesterol-rich liposomes have higher drug
15 retention rate compared to cholesterol-free liposomes at temperature below T_c .^{34 35 36} This is
16 probably because the high content of cholesterol can suppress the permeability as rigid "barriers"
17 in the bilayer membrane.³⁷

18 On the other hand, after heated to 75°C (above T_c) for 15 minutes, -Chol +Au liposomes
19 released 137.8 ± 2.6 $\mu\text{g/mL}$ MTX, while +Chol +Au liposomes released 155.3 ± 5.1 $\mu\text{g/mL}$
20 MTX ($p = 0.001$). The result indicated the effect of cholesterol on facilitating drug release above
21 T_c .

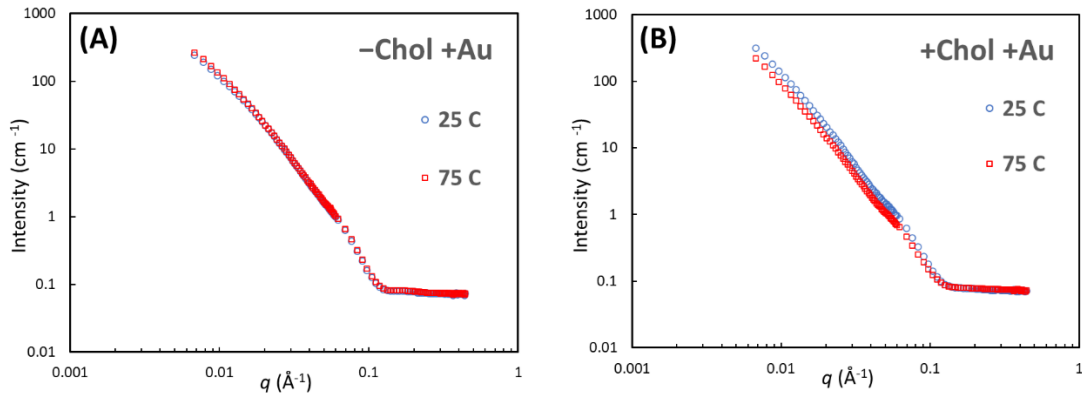
1 However, the effect of cholesterol on the drug release when the whole sample was heated
2 seemed less compared to the 20 s laser-irradiated drug release (Figure 1). The drug release
3 amount from +Chol +Au liposomes was $\sim 20 \mu\text{g/mL}$ more than -Chol +Au by the 15 min heating
4 whereas the difference was $\sim 50 \mu\text{g/mL}$ by 15 second laser irradiation. The results suggest that
5 bulk heating and the laser irradiation shares the drug release mechanism, but not in the exactly
6 the same manner. The effect of heating versus laser can be comparable to the effect of a
7 continuous wave (CW) laser versus pulsed laser on drug release. One study has shown that a
8 femtosecond pulsed laser resulted in higher percentage of drug release than CW at the same laser
9 power and duration.³⁸ The overall temperature increase for the pulsed laser group was lower
10 than the CW laser group. The peak power from the pulsed laser is in fact several orders higher
11 than the CW, leading to effective “melting” of the lipid bilayer locally and specifically only to
12 the liposomes irradiated. Therefore, shorter laser duration with a pulsed laser yields the same
13 amount of drug release compared to CW. In addition, because long exposure to heat can damage
14 healthy tissue by hyperthermia, drug release by the pulsed laser would be advantageous for
15 practical reasons.



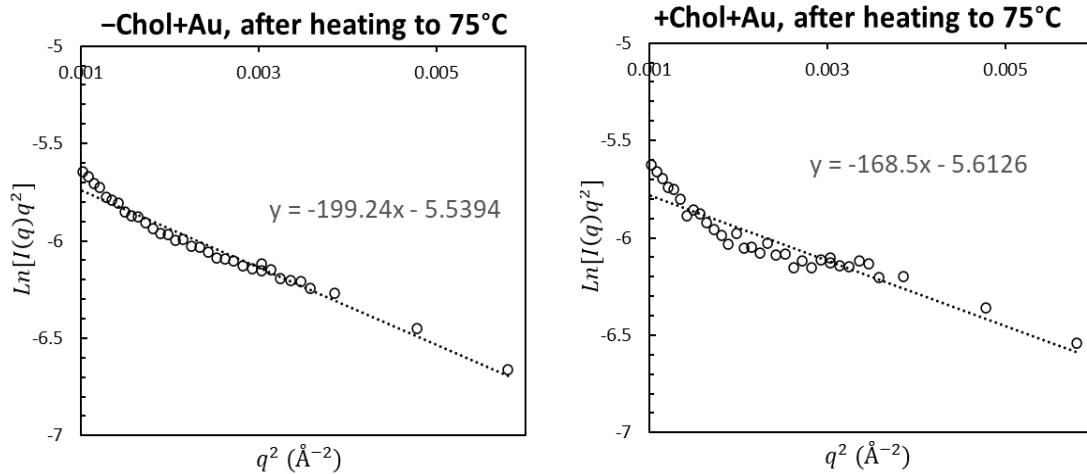
16
17 Figure 7. Effect of temperature on the concentration of released MTX of the -Chol +Au and +Chol +Au
18 liposomes.

19
20 Figure 8 shows SANS data for the liposomes heated above T_c and cooled to room
21 temperature. Similar to the scattering curves of laser-irradiated liposomes (Figure 3), the +Chol
22 +Au curve was shifted to left, whereas -Chol +Au had no changes between before heating and
23 after heating. According to the Kratky-Porod plots shown in Figure 9, the bilayer thickness for

1 heated -Chol +Au and heated +Chol +Au liposomes were determined to be 4.9 ± 0.1 nm and 4.5
 2 ± 0.2 (Table 4), respectively. It is close to the original thickness prior to heating. The heating
 3 temperature of 75°C was not able to induce melting or deformation of AuNRs. Therefore, the
 4 differences in scattering curves only represents a structural change of liposomes.



5
 6 Figure 8. EQ-SANS scattering curves for (A) -Chol +Au liposomes after heated to 75°C for 20 min and
 7 cooled to room temperature, (B) +Chol +Au liposomes after heated to 75°C for 20 min and cooled to
 8 room temperature.



9
 10 Figure 9. The Kratky-Porod plots of the SANS scattering data for (A) -Chol +Au and (B)+Chol +Au
 11 liposomes after heated to 75°C and cooled to room temperature. Dashed lines are the trendlines of linear
 12 fittings.

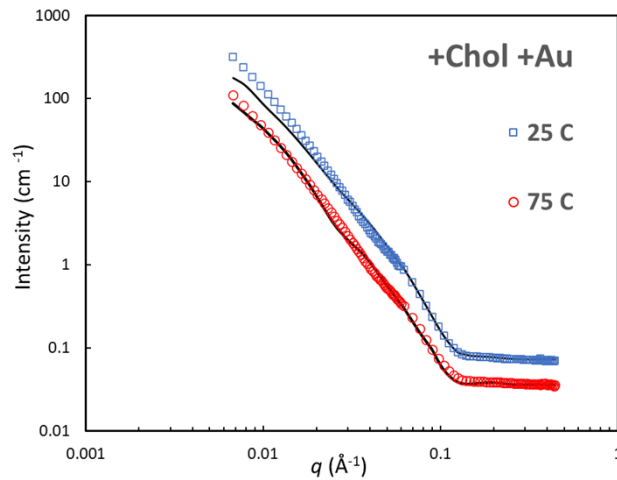
13 As validated in the previous section, the customized model was used to fit the data for
 14 +Chol +Au heating to 75°C (Figure 10). Similarly, we used a second core-shell-sphere model

1 representing the aggregated liposomes to quantify the changes. Table 5 summarizes the
2 parameters associated with the fittings shown in Figure 10. The fitting results show that, after
3 heating, about 29% of liposomes transformed to aggregates with a radius of ~155 nm.

4

5 Table 4. Parameters of the lipid bilayers for liposomes with heating obtained from the Kratky-Porod plots.

Composition	Condition	R_t^2 (nm ²)	d_t (nm)
-Chol +Au	Heated to 75C	2.0 ± 0.1	4.9 ± 0.1
+Chol +Au	Heated to 75C	1.7 ± 0.1	4.5 ± 0.2



6

7 Figure 10. EQ-SANS scattering curves for +Chol +Au liposomes after heated to 75°C for 20 min and
8 cooled to room temperature. Solid black lines represent the fitting curve. The scattering curve has been
9 shifted for better illustration.

10

11

12

13

14

15

1 Table 5. Fitting models and parameters for the +Chol +Au liposomes without heating (25°C), +Chol +Au
 2 liposomes after heating to 75°C and cooled down, respectively.

Sample	Component (model)	d_t (nm)	R_{core} (nm)	PD	Scale	Percentage of liposome/aggregate
+Chol +Au, 25°C (no heating)	Core-shell-sphere (liposome)	4.3	51	0.27	0.060	100%
	Cylinder (AuNR)	Radius × Length: 13 × 132		0.14 (radius) 0.20 (length)	0.005	
+Chol +Au, heated to 75°C then cooled down	Core-shell-sphere (liposome)	4.5	51	0.4	0.042	71% liposome 29% aggregate
	Core-shell-sphere (aggregate)	4.5	155	0.4	0.018	
	Cylinder (AuNR)	Radius × Length: 13 × 132		0.14 (radius) 0.20 (length)	0.005	

3

4 4. Conclusions

5 In this study, we found that inclusion of 35 mol% cholesterol (+Chol +Au) remarkably
 6 facilitated the drug release of laser-activated liposomes. In contrast, the cholesterol-free
 7 liposomes (−Chol +Au) barely released drug at the same laser conditions. The TEM results and
 8 the SANS data showed an aggregation or fusion only for the +Chol +Au liposomes after
 9 irradiation, indicating cholesterol played an important role in changing lipid bilayer membrane
 10 affecting aggregation during and after laser irradiation, resulting in drug release through the
 11 membrane. However, the Kratky-Porod plot analysis suggested the lipid bilayer thickness did not
 12 change. In addition, heating experiments confirmed more drug release with cholesterol in the
 13 lipid composition than in the absence of cholesterol, suggesting cholesterol enhances fluidity at
 14 temperature above chain-transition temperature T_c . Overall, the study revealed two important
 15 findings: (1) inclusion of 35 mol% cholesterol enhanced the permeability of lipid bilayers above
 16 T_c ; (2) the mechanism of laser-activated liposomal drug delivery is disrupting lipid bilayer
 17 membranes by the photothermal effect in the presence of plasmonic materials. By understanding
 18 the fundamentals of the technology, more precise controlled drug release at a targeted site with
 19 great stability and repeatability is expected.

20

1 References

- 2 (1) Gregoriadis, G. Drug entrapment in liposomes. *FEBS letters* **1973**, *36* (3), 292-296.
- 3 (2) Riaz, M. Liposomes preparation methods. *Pakistan journal of pharmaceutical sciences* **1996**,
4 *9* (1), 65-77.
- 5 (3) Berger, N.; Sachse, A.; Bender, J.; Schubert, R.; Brandl, M. Filter extrusion of liposomes
6 using different devices: comparison of liposome size, encapsulation efficiency, and process
7 characteristics. *Int J Pharm* **2001**, *223* (1-2), 55-68. DOI: 10.1016/s0378-5173(01)00721-9
8 From NLM.
- 9 (4) Szoka, F.; Papahadjopoulos, D. Procedure for preparation of liposomes with large internal
10 aqueous space and high capture by reverse-phase evaporation. *Proceedings of the national
11 academy of sciences* **1978**, *75* (9), 4194-4198.
- 12 (5) Shi, N.-Q.; Qi, X.-R. Preparation of Drug Liposomes by Reverse-Phase Evaporation. In
13 *Liposome-Based Drug Delivery Systems*, Lu, W.-L., Qi, X.-R. Eds.; Springer Berlin Heidelberg,
14 2021; pp 37-46.
- 15 (6) Chaves, M. A.; Baldino, L.; Pinho, S. C.; Reverchon, E. Supercritical CO₂ assisted process
16 for the production of mixed phospholipid nanoliposomes: Unloaded and vitamin D₃-loaded
17 vesicles. *Journal of Food Engineering* **2022**, *316*, 110851.
- 18 (7) William, B.; Noémie, P.; Brigitte, E.; Géraldine, P. Supercritical fluid methods: An
19 alternative to conventional methods to prepare liposomes. *Chemical Engineering Journal* **2020**,
20 *383*, 123106. DOI: <https://doi.org/10.1016/j.cej.2019.123106>.
- 21 (8) Lindner, L.; Hossann, M. Factors affecting drug release from liposomes. *Current opinion in
22 drug discovery & development* **2010**, *13*, 111-123.
- 23 (9) Bozzuto, G.; Molinari, A. Liposomes as nanomedical devices. *International journal of
24 nanomedicine* **2015**, *10*, 975-999. DOI: 10.2147/IJN.S68861 PubMed.
- 25 (10) Rwei, A. Y.; Wang, B. Y.; Ji, T.; Zhan, C.; Kohane, D. S. Enhanced triggering of local
26 anesthetic particles by photosensitization and photothermal effect using a common wavelength.
27 *Nano letters* **2017**, *17* (11), 7138-7145.
- 28 (11) Xing, S.; Zhang, X.; Luo, L.; Cao, W.; Li, L.; He, Y.; An, J.; Gao, D. Doxorubicin/gold
29 nanoparticles coated with liposomes for chemo-photothermal synergetic antitumor therapy.
30 *Nanotechnology* **2018**, *29* (40), 405101.
- 31 (12) Liu, Y.; Zhang, X.; Luo, L.; Li, L.; Zhu, R. Y.; Li, A.; He, Y.; Cao, W.; Niu, K.; Liu, H.
32 Gold-nanobranched-shell based drug vehicles with ultrahigh photothermal efficiency for chemo-
33 photothermal therapy. *Nanomedicine: Nanotechnology, Biology and Medicine* **2019**, *18*, 303-
34 314.
- 35 (13) Liu, K.-C.; Arivajigane, A.; Wu, S.-J.; Tzou, S.-C.; Chen, C.-Y.; Wang, Y.-M.
36 Development of a novel thermal-sensitive multifunctional liposome with antibody conjugation to
37 target EGFR-expressing tumors. *Nanomedicine: Nanotechnology, Biology and Medicine* **2019**,
38 *15* (1), 285-294.
- 39 (14) Paasonen, L.; Sipilä, T.; Subrizi, A.; Laurinmäki, P.; Butcher, S. J.; Rappolt, M.; Yaghmur,
40 A.; Urtti, A.; Yliperttula, M. Gold-embedded photosensitive liposomes for drug delivery:
41 triggering mechanism and intracellular release. *Journal of Controlled Release* **2010**, *147* (1),
42 136-143. Hwang, S.; Nam, J.; Jung, S.; Song, J.; Doh, H.; Kim, S. Gold nanoparticle-mediated
43 photothermal therapy: current status and future perspective. *Nanomedicine* **2014**, *9* (13), 2003-
44 2022. Forbes, N.; Pallaoro, A.; Reich, N. O.; Zasadzinski, J. A. Rapid, reversible release from

1 thermosensitive liposomes triggered by near-infra-red light. *Particle & Particle Systems*
2 *Characterization* **2014**, *31* (11), 1158-1167.
3 (15) Chen, W.; Goldys, E. M.; Deng, W. Light-induced liposomes for cancer therapeutics.
4 *Progress in Lipid Research* **2020**, *79*, 101052. DOI:
5 <https://doi.org/10.1016/j.plipres.2020.101052>.
6 (16) Briuglia, M.-L.; Rotella, C.; McFarlane, A.; Lamprou, D. A. Influence of cholesterol on
7 liposome stability and on in vitro drug release. *Drug Delivery and Translational Research* **2015**,
8 *5* (3), 231-242. DOI: 10.1007/s13346-015-0220-8. Zhao, Y.; Dai, X.; Wei, X.; Yu, Y.; Chen, X.;
9 Zhang, X.; Li, C. Near-Infrared Light-Activated Thermosensitive Liposomes as Efficient Agents
10 for Photothermal and Antibiotic Synergistic Therapy of Bacterial Biofilm. *ACS Applied*
11 *Materials & Interfaces* **2018**, *10* (17), 14426-14437. DOI: 10.1021/acsami.8b01327. Barenholz,
12 Y. Doxil® — The first FDA-approved nano-drug: Lessons learned. *Journal of Controlled*
13 *Release* **2012**, *160* (2), 117-134. DOI: <https://doi.org/10.1016/j.jconrel.2012.03.020>.
14 (17) Das, S.; Lazenby, R. A.; Yuan, Z.; White, R. J.; Park, Y. C. Effect of Laser Irradiation on
15 Reversibility and Drug Release of Light-Activatable Drug-Encapsulated Liposomes. *Langmuir*
16 **2020**, *36* (13), 3573-3582.
17 (18) Yuan, Z.; Das, S.; Lazenby, R. A.; White, R. J.; Park, Y. C. Repetitive drug releases from
18 light-activatable micron-sized liposomes. *Colloids and Surfaces A: Physicochemical and*
19 *Engineering Aspects* **2021**, *625*, 126778.
20 (19) Inoue, K. Permeability properties of liposomes prepared from dipalmitoyllecithin,
21 dimyristoyllecithin, egg lecithin, rat liver lecithin and beef brain sphingomyelin. *Biochimica et*
22 *Biophysica Acta (BBA)-Biomembranes* **1974**, *339* (3), 390-402.
23 (20) Anderson, M.; Omri, A. The effect of different lipid components on the in vitro stability and
24 release kinetics of liposome formulations. *Drug delivery* **2004**, *11* (1), 33-39.
25 (21) Arriaga, L. R.; López-Montero, I.; Monroy, F.; Orts-Gil, G.; Farago, B.; Hellweg, T.
26 Stiffening effect of cholesterol on disordered lipid phases: a combined neutron spin echo+
27 dynamic light scattering analysis of the bending elasticity of large unilamellar vesicles.
28 *Biophysical journal* **2009**, *96* (9), 3629-3637.
29 (22) Zhao, L.; Temelli, F.; Curtis, J. M.; Chen, L. Preparation of liposomes using supercritical
30 carbon dioxide technology: Effects of phospholipids and sterols. *Food Research International*
31 **2015**, *77*, 63-72.
32 (23) Abràmoff, M. D.; Magalhães, P. J.; Ram, S. J. Image processing with ImageJ. *Biophotonics*
33 *international* **2004**, *11* (7), 36-42.
34 (24) Jang, Y.; Choi, W. T.; Heller, W. T.; Ke, Z.; Wright, E. R.; Champion, J. A. Engineering
35 globular protein vesicles through tunable self-assembly of recombinant fusion proteins. *Small*
36 **2017**, *13* (36), 1700399.
37 (25) Owoseni, O.; Zhang, Y.; Omarova, M.; Li, X.; Lal, J.; McPherson, G. L.; Raghavan, S. R.;
38 Bose, A.; John, V. T. Microstructural characteristics of surfactant assembly into a gel-like
39 mesophase for application as an oil spill dispersant. *Journal of colloid and interface science*
40 **2018**, *524*, 279-288.
41 (26) García, M. C.; Naitlho, N.; Calderón-Montaña, J. M.; Drago, E.; Rueda, M.; Longhi, M.;
42 Rabasco, A. M.; López-Lázaro, M.; Prieto-Dapena, F.; González-Rodríguez, M. L. Cholesterol
43 Levels Affect the Performance of AuNPs-Decorated Thermo-Sensitive Liposomes as
44 Nanocarriers for Controlled Doxorubicin Delivery. *Pharmaceutics* **2021**, *13* (7), 973.

- 1 (27) Shin, J. E.; Ogunyankin, M. O.; Zasadzinski, J. A. Near Infrared-Triggered Liposome Cages
2 for Rapid, Localized Small Molecule Delivery. *Scientific reports* **2020**, *10* (1), 1-11.
- 3 (28) Ogunyankin, M. O.; Shin, J. E.; Lapotko, D. O.; Ferry, V. E.; Zasadzinski, J. A. Optimizing
4 the NIR fluence threshold for nanobubble generation by controlled synthesis of 10–40 nm
5 hollow gold nanoshells. *Advanced functional materials* **2018**, *28* (10), 1705272.
- 6 (29) Gallová, J.; Uhríková, D.; Kučerka, N.; Doktorovová, S.; Funari, S. S.; Teixeira, J.;
7 Balgavý, P. The effects of cholesterol and β -sitosterol on the structure of saturated
8 diacylphosphatidylcholine bilayers. *European Biophysics Journal* **2011**, *40* (2), 153-163.
- 9 (30) Kratky, O.; Porod, G. Röntgenuntersuchung gelöster fadenmoleküle. *Recueil des Travaux*
10 *Chimiques des Pays-Bas* **1949**, *68* (12), 1106-1122.
- 11 (31) Marra, J.; Israelachvili, J. Direct measurements of forces between phosphatidylcholine and
12 phosphatidylethanolamine bilayers in aqueous electrolyte solutions. *Biochemistry* **1985**, *24* (17),
13 4608-4618.
- 14 (32) McIntosh, T. J. The effect of cholesterol on the structure of phosphatidylcholine bilayers.
15 *Biochimica et Biophysica Acta (BBA)-Biomembranes* **1978**, *513* (1), 43-58.
- 16 (33) Nigro, V.; Angelini, R.; King, S.; Franco, S.; Buratti, E.; Bomboi, F.; Mahmoudi, N.;
17 Corvasce, F.; Scaccia, R.; Church, A. Apparatus for simultaneous dynamic light scattering–small
18 angle neutron scattering investigations of dynamics and structure in soft matter. *Review of*
19 *Scientific Instruments* **2021**, *92* (2), 023907.
- 20 (34) Ogihara-Umeda, I.; Kojima, S. Cholesterol enhances the delivery of liposome-encapsulated
21 gallium-67 to tumors. *European journal of nuclear medicine* **1989**, *15* (9), 612-617.
- 22 (35) Senior, J.; Gregoriadis, G. Stability of small unilamellar liposomes in serum and clearance
23 from the circulation: the effect of the phospholipid and cholesterol components. *Life sciences*
24 **1982**, *30* (24), 2123-2136.
- 25 (36) Deniz, A.; Sade, A.; Severcan, F.; Keskin, D.; Tezcaner, A.; Banerjee, S. Celecoxib-loaded
26 liposomes: effect of cholesterol on encapsulation and in vitro release characteristics. *Bioscience*
27 *reports* **2010**, *30* (5), 365-373.
- 28 (37) Needham, D.; McIntosh, T.; Evans, E. Thermomechanical and transition properties of
29 dimyristoylphosphatidylcholine/cholesterol bilayers. *Biochemistry* **1988**, *27* (13), 4668-4673.
- 30 Needham, D.; Nunn, R. S. Elastic deformation and failure of lipid bilayer membranes containing
31 cholesterol. *Biophysical journal* **1990**, *58* (4), 997-1009. Bloom, M.; Evans, E.; Mouritsen, O. G.
32 Physical properties of the fluid lipid-bilayer component of cell membranes: a perspective.
33 *Quarterly reviews of biophysics* **1991**, *24* (3), 293-397.
- 34 (38) Sahu, A.; Kim, M.; Ryu, J.; Son, J.-G.; Lee, E.; Noh, D. Y.; Tae, G. Nanographene oxide as
35 a switch for CW/pulsed NIR laser triggered drug release from liposomes. *Material Science and*
36 *Engineering* **2018**, *82*, 5.

37